



Power Electronic Systems
Laboratory

© 2013 IEEE

Proceedings of the 10th IEEE International Conference on Power Electronics and Drive Systems (PEDS 2013), Kitakyushu, Japan, April 22-25, 2013

Medium Frequency Transformers for Solid-State-Transformer Applications - Design and Experimental Verification

G. Ortiz,
M. Leibl,
J. W. Kolar,
O. Apeldoorn

This material is published in order to provide access to research results of the Power Electronic Systems Laboratory / D-ITET / ETH Zurich. Internal or personal use of this material is permitted. However, permission to reprint/republish this material for advertising or promotional purposes or for creating new collective works for resale or redistribution must be obtained from the copyright holder. By choosing to view this document, you agree to all provisions of the copyright laws protecting it.



Eidgenössische Technische Hochschule Zürich
Swiss Federal Institute of Technology Zurich

Medium Frequency Transformers for Solid-State-Transformer Applications - Design and Experimental Verification

G. Ortiz*, M. Leibl*, J. W. Kolar* and O. Apeldoorn**

*Power Electronic Systems Laboratory, ETH Zurich

**Power Electronics and Medium Voltage Drives, ABB Switzerland AG

Email: ortiz@lem.ee.ethz.ch

Abstract—Solid-state-transformer technology pushes the specifications of electric transformers in the high-power medium-frequency range. This combination results in larger-sized transformers operating at higher frequencies whereby parasitic phenomenon should be carefully accounted for. This paper presents an analytical description of the limiting factors and the connection between frequency/power rating and the available core and copper conductor technology on the power density and efficiency of medium-frequency transformers. Furthermore, two designed transformers for 166 kW/20 kHz based on two different core materials and cooling systems are presented. Extensive copper, core and cooling system loss measurements on one of these transformers are discussed in order to analyze the transformers' behavior from a practical point of view.

I. INTRODUCTION

Electric transformers, either utilized in electric power systems or within a power electronic-based converter, are fundamental components within modern high-efficient energy supply chains. Two important specifications of these transformers are their VA (power) rating and operating frequency since, combined with the available magnetic core materials and copper conductor technology, they strongly influence the two key features of a transformer: its efficiency and power-density.

Depending on their VA/frequency ratings, transformers can be classified into four main groups, as shown in Fig. 1. For high power levels > 50 kW line frequency, i.e. 50 Hz or 60 Hz transformers are the predominant choice (e.g. for distribution applications) due to their simplicity and comparatively high efficiency. At lower powers < 50 kW, low frequency 50 Hz transformers can be found mainly at the input of isolated power supplies with low power density requirements. Power electronics circuits enable the operation of transformers at higher frequencies, thus facilitating the realization of highly-compact and high-efficiency power supplies, as described in the literature for power levels up to 50 kW [1].

Driven mainly by the growing interests in Smart Grid technologies and modern traction solutions and enabled by recent advances in semiconductor devices operated under soft-switching modulation schemes, systems of higher power > 50 kW with DC-DC converters operating at Medium Frequency (MF) > 1 kHz are currently subject to strong attention [2]. In particular, the Solid-State-Transformer (SST) concept combines the desired features of flexible power routing [3] (smart-grids) due to the mains and load side active power circuits and the reduction in size/weight due to the operation

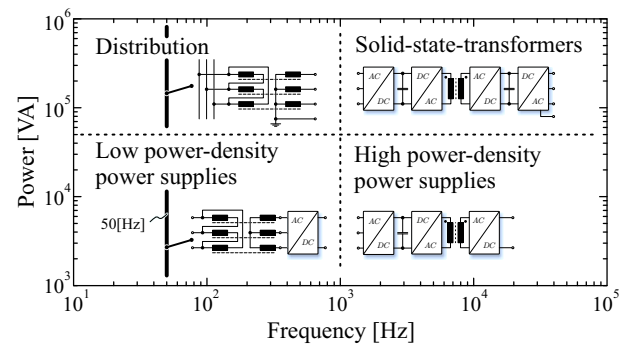


Figure 1: Classification of electric transformers based on their power/frequency specifications.

at MF of the isolation transformer (attractive for modern traction solutions) [4–6].

From the transformer's perspective, for a given operating frequency, higher power leads to an increased size. However, the combination of higher frequencies and larger dimensions results in strong parasitic effects in the core material, copper conductors and, in some cases, in the cooling system. If not properly accounted for, these effects increase the losses of the transformer, decreasing its efficiency and ultimately compromising its reliability. Moreover, for a given efficiency, higher power density leads to higher loss density, thus efficient transformer cooling concepts become mandatory.

This paper explores by means of Pareto-front analysis the trade-offs present in the construction of MF transformers starting from a theoretical analysis of the boundaries in power density and efficiency imposed by today's available core materials and copper conductor technology in **Section II**. Practical considerations are included in the optimized design of two transformer examples realized with different core materials and cooling concepts, as described in **Section III**. Details about the realization of these two transformers and exhaustive measurement results are presented in **Section IV**.

II. LIMITS OF HIGH-POWER MF TRANSFORMERS

Inductive components are ideally designed such that power density and efficiency are in Pareto optimum. This means that the power density can not be increased without reducing efficiency. All Pareto optimal pairs of power density and efficiency compose a line, called the Pareto front. In this section it is shown, that for a certain transformer design there is a optimum frequency that maximizes efficiency and power density. The apparent power S of a transformer is given as:

$$S = \frac{\omega \hat{B} \hat{J} A_c A_w}{4} \quad (1)$$

With the core and winding areas A_c , A_w , the spatial average of flux density and current density amplitudes \hat{B} , \hat{J} and the frequency $\omega = 2\pi f$.

The core loss density can be calculated by the original Steinmetz equation:

$$p_c = k_{f_e}^{1-\beta} k f^\alpha \hat{B}^\beta \quad (2)$$

With core filling factor k_{f_e} and the Steinmetz parameters k , α and β of the core material.

The loss density of a litz wire winding results from the approximation for strand diameters smaller than skin depth [7] and assuming a one dimensional magnetic field distribution as it would result from homogenously distributed strands in the core window.

$$p_w = \frac{1}{k_{cu}\sigma} (1 + af^2) \frac{\hat{J}^2}{2} \quad (3)$$

With $a = \frac{1}{48} (\pi k_{cu} \sigma \mu w_w d_s)^2$, the winding filling factor k_{cu} , the conductivity σ , the winding width w_w and the strand diameter d_s .

It is now assumed, that all geometric dimensions of a transformer, the strand diameter and the core material are given. Further, the transformer is initially operated at a frequency f_0 , a flux density \hat{B}_0 and a current density \hat{J}_0 . A variation of f , \hat{B} and \hat{J} results in relative changes in apparent power and core and winding loss densities:

$$\frac{S}{S_0} = \frac{f \hat{B} \hat{J}}{f_0 \hat{B}_0 \hat{J}_0} \quad (4)$$

$$\frac{p_c}{p_{c0}} = \left(\frac{f}{f_0}\right)^\alpha \left(\frac{\hat{B}}{\hat{B}_0}\right)^\beta \quad (5)$$

$$\frac{p_w}{p_{w0}} = \frac{(1 + af^2) \hat{J}^2}{(1 + af_0^2) \hat{J}_0^2} \quad (6)$$

We will now set the relative change in apparent power equal to each relative change in loss density, i.e. we set $\frac{S}{S_0} = \frac{p_c}{p_{c0}}$ and $\frac{S}{S_0} = \frac{p_w}{p_{w0}}$. Which means that the efficiency is kept constant. Each expressions yields the rise in current density:

$$\frac{\hat{J}}{\hat{J}_0} = \left(\frac{f}{f_0}\right)^{\alpha-1} \left(\frac{\hat{B}}{\hat{B}_0}\right)^{\beta-1} \quad (7)$$

$$\frac{\hat{J}}{\hat{J}_0} = \frac{f \hat{B} (1 + af_0^2)}{f_0 \hat{B}_0 (1 + af^2)} \quad (8)$$

From equating (7) and (8) we find the relative change of the flux density with frequency:

$$\frac{\hat{B}}{\hat{B}_0} = \left(\frac{f}{f_0}\right)^{\frac{2-\alpha}{\beta-2}} \left(\frac{1 + af_0^2}{1 + af^2}\right)^{\frac{1}{\beta-2}} \quad (9)$$

And by inserting (9) in (7) or (8) we get the relative change of the current density with frequency:

$$\frac{\hat{J}}{\hat{J}_0} = \left(\frac{f}{f_0}\right)^{\frac{\beta-\alpha}{\beta-2}} \left(\frac{1 + af_0^2}{1 + af^2}\right)^{\frac{\beta-1}{\beta-2}} \quad (10)$$

By inserting (9) and (10) in (4), we obtain the relative change of the apparent power:

$$\frac{S}{S_0} = \left(\frac{f}{f_0}\right)^{\frac{2\beta-2\alpha}{\beta-2}} \left(\frac{1 + af_0^2}{1 + af^2}\right)^{\frac{\beta}{\beta-2}} \quad (11)$$

Independent of f_0 , the apparent power always reaches a maximum at a certain frequency, that only depends on α , β of the core material, the winding conductivity σ , filling factor k_{cu} , the strand diameter d_s and the winding width w_w . This optimum frequency f_{opt} is obtained from differentiating (11) and setting it to zero:

$$f_{opt} = \sqrt{\frac{1}{a} \left(\frac{\beta}{\alpha} - 1\right)} \quad (12)$$

Since the efficiency is kept constant and the power density has a maximum at the frequency f_{opt} , any variation of the frequency would lead to a sub-optimum design. Therefore the optimum frequency criterion is a necessary criterion for Pareto optimality. However, usually the frequency is fixed. In this case one can fulfill the optimum frequency criterion by setting the strand diameter and winding width accordingly.

To set the optimum ratio between current density and flux density for a specific value of apparent power, we start from the total losses of the transformer:

$$P_v = V_c k_c \hat{B}^\beta + V_w k_w \hat{J}^2 \quad (13)$$

With the volume of the core V_c , the volume of the winding V_w , a core loss constant $k_c = k_{f_e}^{1-\beta} k f_{opt}^\alpha$, and a winding loss constant $k_w = \frac{1}{2k_{cu}\sigma} (1 + af^2)$. By expressing and inserting the current density from (1), we find the flux density that minimizes the losses:

$$\hat{B} = \left(\frac{32k_w}{\beta\omega^2 k_c}\right)^{\frac{1}{\beta+2}} S^{\frac{2}{\beta+2}} \left(\frac{V_w}{V_c A_c^2 A_w^2}\right)^{\frac{1}{\beta+2}} \quad (14)$$

Inserting \hat{B} in (13), shows, if the product of strand diameter and winding width is kept constant, that the losses for a certain volume always show a minimum at certain aspect ratios of core and winding area ($p_c = 3.1, p_w = 2.6$), and at a ratio of core width over winding width ($p_{cw} = 1.4$). Using these proportions all geometric dimensions can be calculated from the total volume V_{box} .

In order to obtain a Pareto front, we will now sweep over the strand diameter from 20 μm to 500 μm , the frequency from 8 kHz to 300 kHz and the rated power from 100 W to 10 MW. Only the core materials EPCOS N87 and VAC Vitroperm 500F with their according filling factors are considered, further a winding filling factor of 20% is assumed. The winding width is set such that the optimum frequency criterion is satisfied. Using the aforementioned proportions, the total volume V_{box} and the losses are calculated for the full range of f , d_s and S . The effect of frequency, rated power and cooling system capability on the performance in

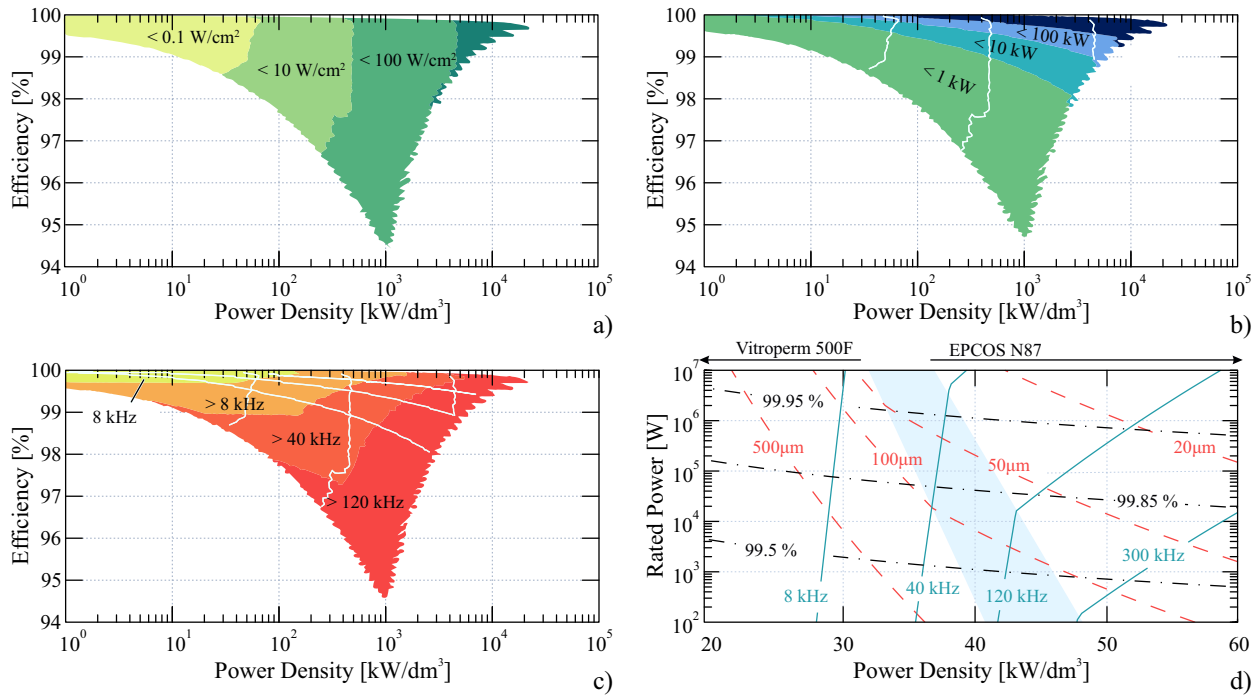


Figure 2: Resulting performance space for a sweep on the parameter range $f = [8 \text{ kHz}, 300 \text{ kHz}]$, $d_s = [20 \mu\text{m}, 500 \mu\text{m}]$, $S = [100 \text{ W}, 10 \text{ MW}]$. V_{box} is adjusted such that all points meet the optimum frequency criterion. a) Average heat flux density on the transformer surface; b) Partitioning of performance space by rated power, the surface loss density levels are indicated as white lines; c) Minimum frequency found on different sections of the performance space. Levels of rated power and heat flux density are indicated as white lines; d) Surface heat flux density is set to 0.1 W/cm^2 , which is possible to reach with natural convection. For a certain rated power and power density one can read the necessary values for strand diameter and frequency, the resulting efficiency and the preferred core material. On the left side of the diagram Vitroperm 500F allows lower switching frequency and higher strand diameter and is therefore the preferred choice. On the right side, EPCOS N87 is favourable for the same reason. In the middle (shaded area), N87 allows higher strand diameter, but F500 allows lower frequency.

terms of power density and efficiency is now investigated. From Fig. 2-a) it can be deduced that for power densities $> 40 \text{ kW/dm}^3$ the design of a cooling system that also meets the isolation requirements is one of the main challenges. The required frequency to reach a certain level of power density depends on the rated power (Figs. 2-b) and c)). Increase in rated power reduces the required frequency and increases the efficiency, but demands a lower strand diameter (Fig. 2-d)).

It should be noted that the aforementioned optimal design does not explicitly take into consideration other practical aspects such as isolation, cooling system geometry or other limitations coming from the power electronic converters such as operating frequencies and rated voltages. These practical aspects will be included in the design of two transformers which will be presented in the following section.

III. OPTIMIZED DESIGN EXAMPLES

The previous analysis is intended to show the theoretical limits of MF transformers imposed mainly by currently available technology (core materials and copper litz wire conductors) not considering the limits of power-electronic converters. Other restrictions may apply to the complete system when the power-electronic circuits are considered. As an example, in [8] a $1 \text{ MW} / 20 \text{ kHz}$ DC-DC converter was proposed. The frequency specification mainly comes from the limitation imposed by medium voltage fast switching semiconductor devices (namely IGBTs) which typically feature high switching losses.

This $1 \text{ MW} / 20 \text{ kHz}$ converter is divided into modules with nominal power of 166 kW each. The structure of these modules is shown in Fig. 3-a). On the MV side, a 2 kV NPC-based structure is built based on 1.7 kV IGBTs. The MF transformer serves as link between the MV and LV converters, whereby this last one is built using a 400 V DC-link-based full-bridge. The utilized modulation scheme ensures soft switching of all semiconductor devices by shaping the current to a triangular waveform [9], as shown in Fig. 3-b) whereby also the peak currents and voltages are displayed.

Two transformer concepts suitable for the topology and waveforms shown in Figs. 3-a) and b) were designed and optimized with respect to power density and efficiency. The two transformer concepts differ mainly in core material (ferrite and nanocrystalline) as well as in cooling concept (air-cooled and water-cooled). Besides the considerations given in Section II, in this case a detailed model of the cooling system was included and therefore a numerical optimization was required due to the higher complexity of the transformer model¹.

A cross-sectional view of the first designed transformer is shown in Fig. 3-c). This design comprises 20 ferrite N87 U-shaped cores as magnetic material and litz wire with $9500 \cdot 71 \mu\text{m}$ strand diameter where 3 parallel litz wires with two turns each are utilized in the LV side winding whereas the

¹A detailed description of the cooling system's model and the proposed optimization procedure will be matter of future publications

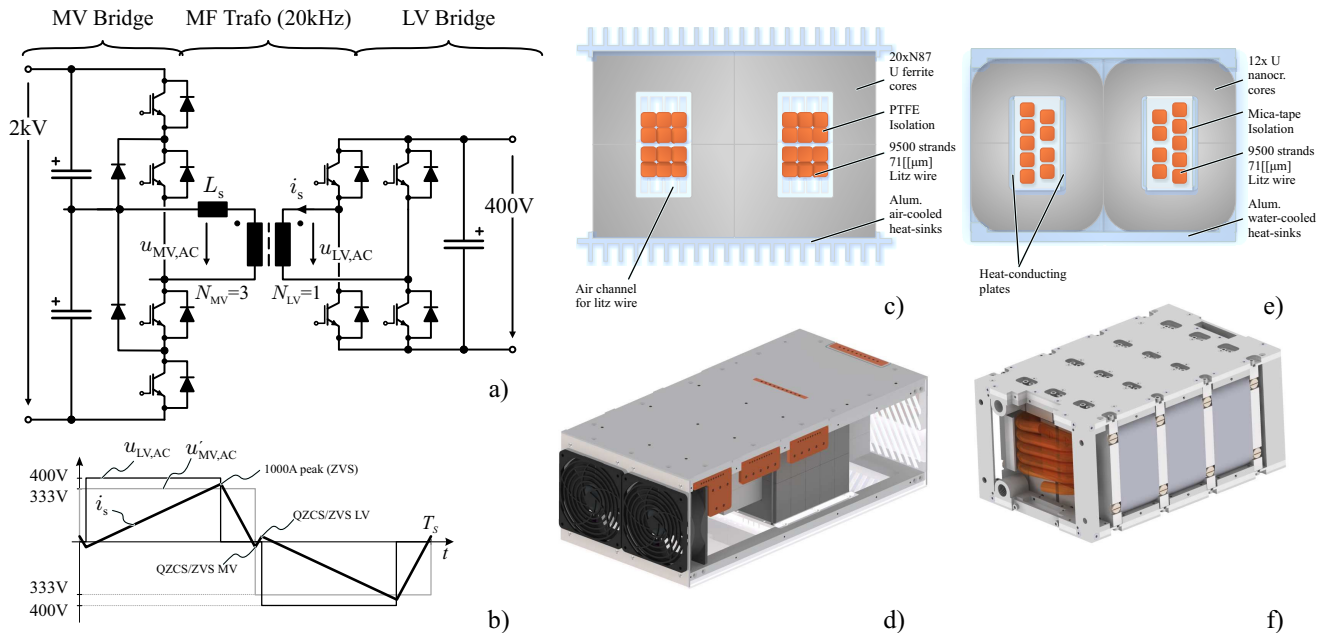


Figure 3: Converter module and designed MF transformers: a) Module structure comprising 3-level NPC bridge on MV side, MF transformer and LV full-bridge; b) Voltage and current waveforms on the MV transformer. The two optimized transformer concepts are based on ferrite and nanocrystalline core materials. The winding arrangement and a CAD drawing of the ferrite-based air-cooled transformer are shown in c) and d) respectively. The respective winding window and CAD drawing for the nanocrystalline-based transformer are shown in e) and f) respectively.

MV side winding is built using 6 turns of the same litz wire. The isolation is provided by a PTFE bobbin and the complete system is cooled by forced convection provided by two front 120 mm fans, as shown in Fig. 3-d). In this case, calculated core and copper losses are 161 W and 230 W respectively.

The second constructed transformer is based on nanocrystalline core material and its winding cross-sectional view is shown in Fig. 3-e). This transformer utilizes the same $9500 \cdot 71 \mu\text{m}$ litz wire whereby two paralleled conductors with 2 turns each are used on the LV side whereas a single wire with 5 turns is utilized on the MV side. The isolation in this case is based on mica tape as often used in electrical machines. The cooling system is based on thermal conduction of heat from winding and core by means of aluminum parts that are attached to two water-cooled heat sinks. The complete arrangement of the transformer including cores and cooling system is shown in Fig. 3-f). More details about the construction of the cooling system will be presented in the next section along with the experimental verification of the calculated losses, which amount to 222 W and 131 W respectively for the core and copper losses respectively. In addition, 20 W were calculated for the cooling system by means of FEM simulations.

Extensive measurements have been performed on these two transformers in order to validate the proposed transformer concepts as well as the calculated core and copper losses. These measurements are outlined in detail in the next section.

IV. EXPERIMENTAL VERIFICATION AND PRACTICAL CONSIDERATIONS

The finally built MF transformers are shown in Figs. 4-a) and b) for the ferrite and nanocrystalline-based transformers

respectively. In order to experimentally verify the calculated values for core and copper losses, these transformers were subject to extensive experimental testing. The focus is placed on the nanocrystalline-based transformer since a verification of the losses in the cooling system is required in this case.

A. Current Sharing in Litz Wire Bundles

The utilized litz wire is based on 10 bundles with 950 litz each. The first test consists of measuring the current in each of these bundles in the nanocrystalline-based transformer in order to quantify the impact of the transformer's size on the current distribution in these bundles. In all cases the current was fed from MV side with a short circuited LV side winding, i.e. only the stray inductance of the transformer limits the conducted current. Also the aluminium cooling system was removed in this case. On the MV side a current of 25 A RMS is fed and the current in each litz wire bundle is measured with a Rogowski coil while the total losses in the winding are measured with a Yokogawa WT3000 precision power analyzer.

For the first test, a termination of the litz wire which ensures same length on all litz wires was adopted. The litz wire was delivered by the manufacturer with two middle non-interchanged bundles (in red) surrounded by 8 bundles with interchanged positions (in blue) as shown in Fig. 5-a). The measured currents can also be seen in Fig. 5-a) together with the schematic view of the litz/termination arrangement. As can be seen, non-interchanged bundles in the middle of the litz wire result in negative circulating currents, increasing the losses in the complete litz wire whereby the AC to DC resistance ratio is $R_{AC}/R_{DC} = 3.01$.

As a second test, the middle non-interchanged conductors were disconnected while keeping the remaining 8 bundles.

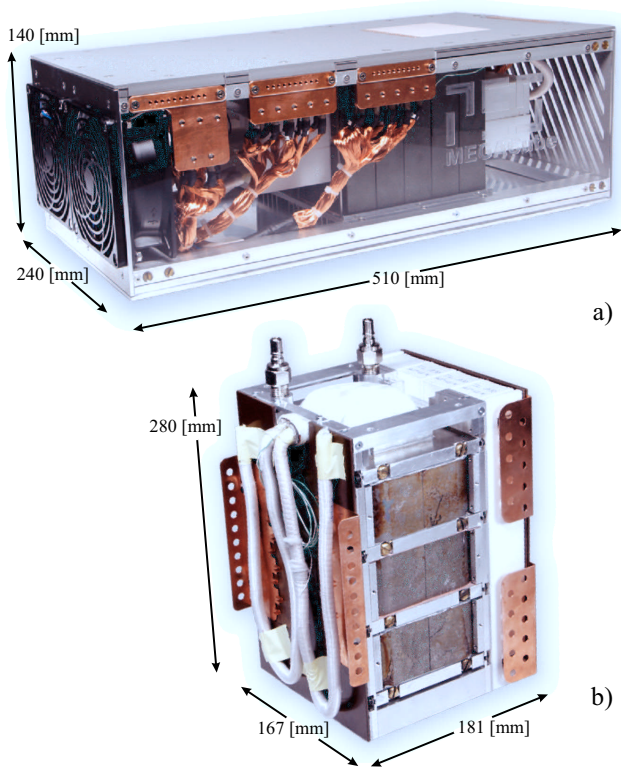


Figure 4: Final assembled 166 kW/20 kHz transformers: a) Ferrite-based air-cooled; b) Nanocrystalline-based water-cooled.

The current sharing in this case is considerably improved as can be seen in Fig. 5-b) whereby the AC to DC resistance ratio is reduced to $R_{AC}/R_{DC} = 1.95$, proving the importance of a symmetrically built litz wire at this frequency/dimensions range.

For practical reasons, the connection of the litz wire to the power-electronic switches is realized by spreading the litz wire bundles into copper plates which are later connected to the power semiconductors. The impact of the asymmetry introduced by this connection is shown in Fig. 5-c). No significant rise in the AC to DC resistance ratio with respect to the symmetric termination is observed. In this case, this ratio has a value of $R_{AC}/R_{DC} = 1.98$.

In order to force the symmetrization of these currents, the arrangement of common mode chokes as shown in Fig. 5-e) can be placed on the litz wire bundles, resulting in considerably symmetric currents in each bundle as seen in Fig. 5-d). In spite this symmetric current distribution the AC to DC resistance ratio is $R_{AC}/R_{DC} = 1.94$, i.e. no considerable improvement in losses was achieved (the losses in the common mode chokes were measured resulting in approx. 5 mW and are therefore negligible in this measurement).

With the winding losses experimentally measured, the total losses including core and cooling system of the nanocrystalline transformer presented in Fig. 4-b) will be now shown in order to obtain the total share of losses in this component.

B. Core Losses

Given the paralleled cores utilized to build the magnetic path in the transformer, potential differences in the air-gaps of each core-pair could cause asymmetries in the generated

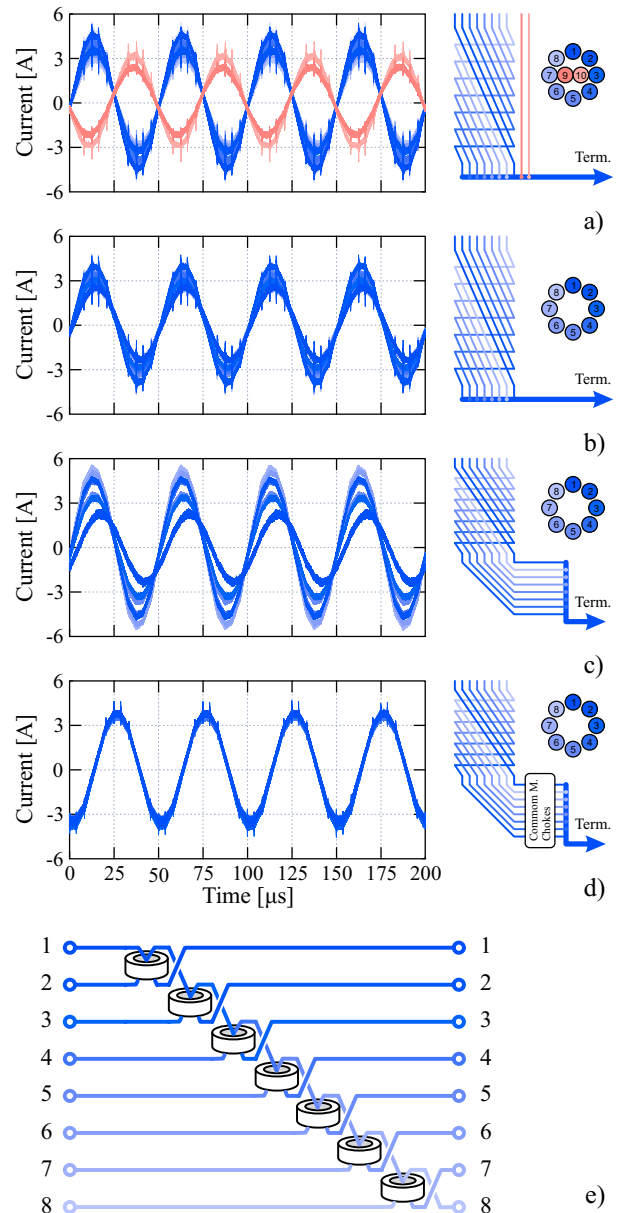


Figure 5: Analysis of current sharing litz wire bundles; a) With middle non-interchanged bundles and symmetric termination; b) Without middle non-interchanged bundles and symmetric termination; c) Without middle non-interchanged bundles and unsymmetric termination; d) Without middle non-interchanged bundles, unsymmetric termination and equalizing common mode chokes (cf. Fig. 5-e); e) Arrangement of common mode chokes to equalize transformer currents.

core losses in each paralleled core. In this case, without a defined air gap, differences of up to 70% in core losses were detected. By introducing an air gap of 0.1 μm between the core pairs, this difference was reduced achieving a decrease of 12% in the total core losses, which are in this case 353 W. The increased losses with respect to calculated values are mainly explained by the un-modeled losses introduced by the cut in tape wound cores [10, 11].

C. Losses in Cooling System

In order to quantify the losses in each part of the cooling system, the increase in losses was measured and therefore the

V. CONCLUSIONS

An analytical expression for the optimum frequency which ensures best use of the available copper and core materials was proposed. With this expression, the impact of various design parameters was studied by means of Pareto front analysis, whereby a clear gain in power density and efficiency is seen when the power of the unit is increased. Additionally the gain in power density attainable with an active cooling system was presented, leading to the two presented ferrite and nanocrystalline-based MF transformers. These two transformers differ in cooling system design, and ultimately in power density.

Experimental measurements were carried out in one of these designed transformers in order to quantify the effect of different parasitic effects in the losses of the system. This analysis confirms the requirement of precise and symmetric fabrication of litz wires and more detailed models which describe the losses in tape wound cores. Furthermore, higher losses in the water-cooling aluminium system designed for the nanocrystalline-based transformer were measured, which indicate the requirement of accurate models for the description of magnetic field distribution in these aluminium parts.

REFERENCES

- [1] M. Pavlovsky, S. W. H. De Haan, and J. Ferreira, "Design for Better Thermal Management in High-Power High-Frequency Transformers," in *Industry Applications Conference, 2005*, vol. 4, Oct. 2005, pp. 2615–2621.
- [2] S. Inoue and H. Akagi, "A Bi-Directional Isolated DC/DC converter as a core circuit of the Next-Generation Medium-Voltage Power Conversion System," in *Power Electronics Specialists Conference, 2006*, June 2006, pp. 1–7.
- [3] J. Wang, A. Huang, W. Sung, Y. Liu, and B. Baliga, "Smart Grid Technologies," *Industrial Electronics Magazine, IEEE*, vol. 3, no. 2, pp. 16–23, 2009.
- [4] D. Dujic, F. Kieferndorf, and F. Canales, "Power Electronics Transformer Technology For Traction Applications - An Overview," *PCIM 2011*, 2011.
- [5] D. Dujic, A. Mester, and T. Chaudhuri, "Laboratory Scale Prototype of a Power Electronic Transformer for Traction Applications," *European Conference on Power Electronics and Applications, 2011*, vol. 1, 2011.
- [6] A. Steimel, "Power-electronic Grid Supply of AC Railway Systems," in *Optimization of Electrical and Electronic Equipment (OPTIM)*, 2012, May 2012, pp. 16–25.
- [7] C. Sullivan, "Optimal Choice for Number of Strands in a Litz-Wire Transformer Winding," in *Power Electronics Specialists Conference, 1997*, vol. 1, 1997, pp. 28–35 vol.1.
- [8] G. Ortiz, J. Biela, D. Bortis, and J. W. Kolar, "1 Megawatt, 20 kHz, Isolated, Bidirectional 12kV to 1.2 kV DC-DC Converter for Renewable Energy Applications," in *IPEC 2010*. IEEE, 2010, pp. 3212–3219.
- [9] G. Ortiz, H. Uemura, D. Bortis, J. Kolar, and O. Apeldoorn, "Modeling of Soft-Switching Losses of IGBTs in High-Power High-Efficiency Dual-Active-Bridge DC/DC converters," *IEEE Transactions on Electron Devices*, vol. 60, no. 2, pp. 587–597, Feb. 2012.
- [10] B. Cougo, A. Tuysu'z, J. Muhlethaler, and J. Kolar, "Increase of Tape Wound Core Losses due to Interlamination Short Circuits and Orthogonal Flux Components," in *IECON 2011*, Nov. 2011, pp. 1372–1377.
- [11] B. Cougo and J. Kolar, "Integration of Leakage Inductance in Tape Wound Core Transformers for Dual Active Bridge Converters," in *International Conference on Integrated Power Electronics Systems (CIPS)*, 2012, March 2012, pp. 1–6.

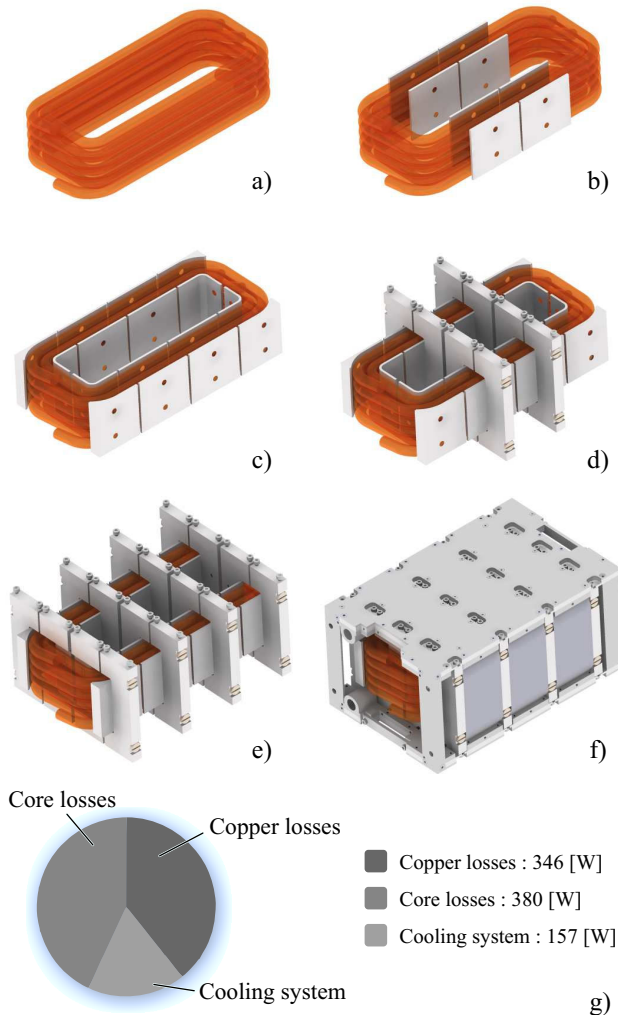


Figure 6: Loss contribution of different transformer cooling parts: a) Pure winding losses; b) Internal cooling plates; c) External cooling plates; d) Internal heat conducting plates; e) External heat conducting plates; f) Top/bottom water-cooled plates; g) Total copper/core/cooling system loss sharing.

source for each of these losses was identified. The different parts of the aluminium cooling system can be seen in Fig. 6 whereby the loss share of each part is:

- Winding, Fig. 6-a) (no cooling system): 353 W
- Internal cooling plates, Fig. 6-b): 56.97 W
- External cooling plates, Fig. 6-c): 18.82 W
- Internal heat conducting plates, Fig. 6-d): 34.28 W
- External heat conducting plates, Fig. 6-e): 44.30 W
- Top/bottom water-cooled plates, Fig. 6-f): 2.83 W

The overall share of copper, core and cooling system losses is presented in Fig. 6-g). The total losses in the cooling system are considerably higher than estimated with FEM simulations (20 W). This phenomena can be explained by different stray field distribution in the winding window due to the effect of the core material lamination and will be analyzed in further publications.